ELSEVIER

CrossMark

Progress in Quantum Electronics 37 (2013) 185–214

Progress in Quantum Electronics

www.elsevier.com/locate/pquantelec

Review

Visible fiber lasers excited by GaN laser diodes

Yasushi Fujimoto[a,*], Jun Nakanishi[b], Tsuyoshi Yamada[b], Osamu Ishii[c], Masaaki Yamazaki[d]

[a]*Institute of Laser Engineering, Osaka University, 2-6 Yamada-oka, Suita, Osaka 565-0871, Japan*
[b]*NIDEK CO., LTD., 34-14 Maehama, Hiroishi-cho, Gamagori, Aichi 443-0038, Japan*
[c]*Production Engineering Section, Optical Glass Production Department, Sumita Optical Glass, Inc., 174-1 Tabehara, Tajima, Minamiaizu-machi, Minamiaizu, Fukushima 967-0004, Japan*
[d]*Glass Research Division, R&D Department, Sumita Optical Glass, Inc., 4-7-25 Harigaya, Urawa-ku, Saitama-City, Saitama 330-8565, Japan*

Available online 16 April 2013

Keywords: Visible fiber laser; AlF_3 system glass; Waterproof property; GaN laser diode; Praseodymium; Dysprosium

Abstract

This paper describes and discusses visible fiber lasers that are excited by GaN laser diodes. One of the attractive points of visible light is that the human eye is sensitive to it between 400 and 700 nm, and therefore we can see applications in display technology. Of course, many other applications exist. First, we briefly review previously developed visible lasers in the gas, liquid, and solid-state phases and describe the history of primary solid-state visible laser research by focusing on rare-earth doped fluoride media, including glasses and crystals, to clarify the differences and the merits of primary solid-state visible lasers. We also demonstrate over 1 W operation of a Pr: WPFG fiber laser due to high-power GaN laser diodes and low-loss optical fibers (0.1 dB/m) made by waterproof fluoride glasses. This new optical fiber glass is based on an AlF_3 system fluoride glass, and its waterproof property is much better than the well known fluoride glass of ZBLAN.

The configuration of primary visible fiber lasers promises highly efficient, cost-effective, and simple laser systems and will realize visible lasers with photon beam quality and quantity, such as high-power CW or tunable laser systems, compact ultraviolet lasers, and low-cost ultra-short pulse laser systems. We believe that primary visible fiber lasers, especially those excited by GaN laser diodes, will be effective tools for creating the next generation of research and light sources.

*Corresponding author. Tel.: +81 6 879 8758; fax: +81 6 877 4799.
E-mail address: fujimoto@ile.osaka-u.ac.jp (Y. Fujimoto).

0079-6727/$ - see front matter © 2013 Elsevier Ltd. All rights reserved.
http://dx.doi.org/10.1016/j.pquantelec.2013.04.002

Contents

1. Introduction

One attractive point of visible light is that we can visualize it. Since the human eye is sensitive to light between 400 and 700 nm, it can discern different wavelengths as colors. Solar irradiance spectra at extraterrestrial and global surfaces are shown in Fig. 1 [1]. The light we see every day is sunlight, which clearly involves the wavelengths that we interpret as colors. Although a relation might be found between the human eye's sensitivity and the spectrum of sunlight at the

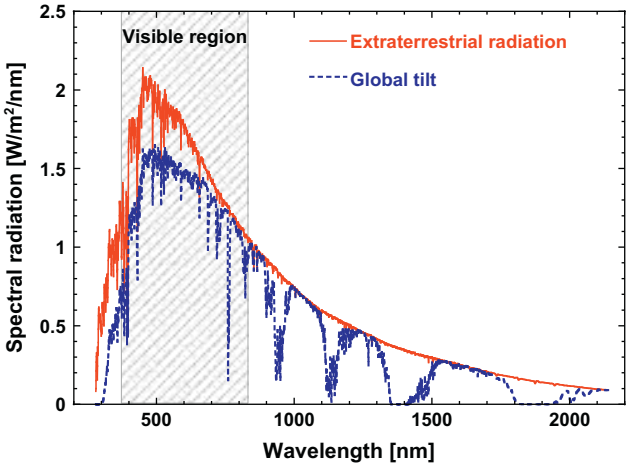

Fig. 1. Solar irradiance spectra at extraterrestrial and global surfaces. Global tilt means spectral radiation from the solar disk plus diffuse sky radiation and diffuse radiation reflected from the ground on the south-facing surface tilted at 37° from the horizontal.

global surface, we will not be addressing that subject in this paper; however, it remains intriguing that knowledge of visible light may increase our understanding of the workings of nature.

Science has obtained two types of light sources so far. One is incoherent light, such as sunlight and halogen lamps; the other is the coherent light source of lasers. In 1917, Einstein published "Quantum theory of radiation" [2] in which he deduced the relation between emission and the absorption of radiation from such important facts in quantum theory as Planck's law of radiation and Wien's displacement law. In 1958, based on Einstein's deduction, Schawlow and Townes provided the theoretical details of infrared and optical masers, which later became known as lasers [3]. In 1960, the ruby laser was created by Maiman [4]. The ruby laser was not only the first laser, but it was also the first visible solid-state laser that emits at 694 nm. Today, we see many lasers at wavelengths between the ultraviolet and infrared that operate in the gas, liquid, and solid-state phases. When compared with incoherent light, lasers have several important characteristics, such as directivity, coherence, and short pulse generation. Therefore, visible

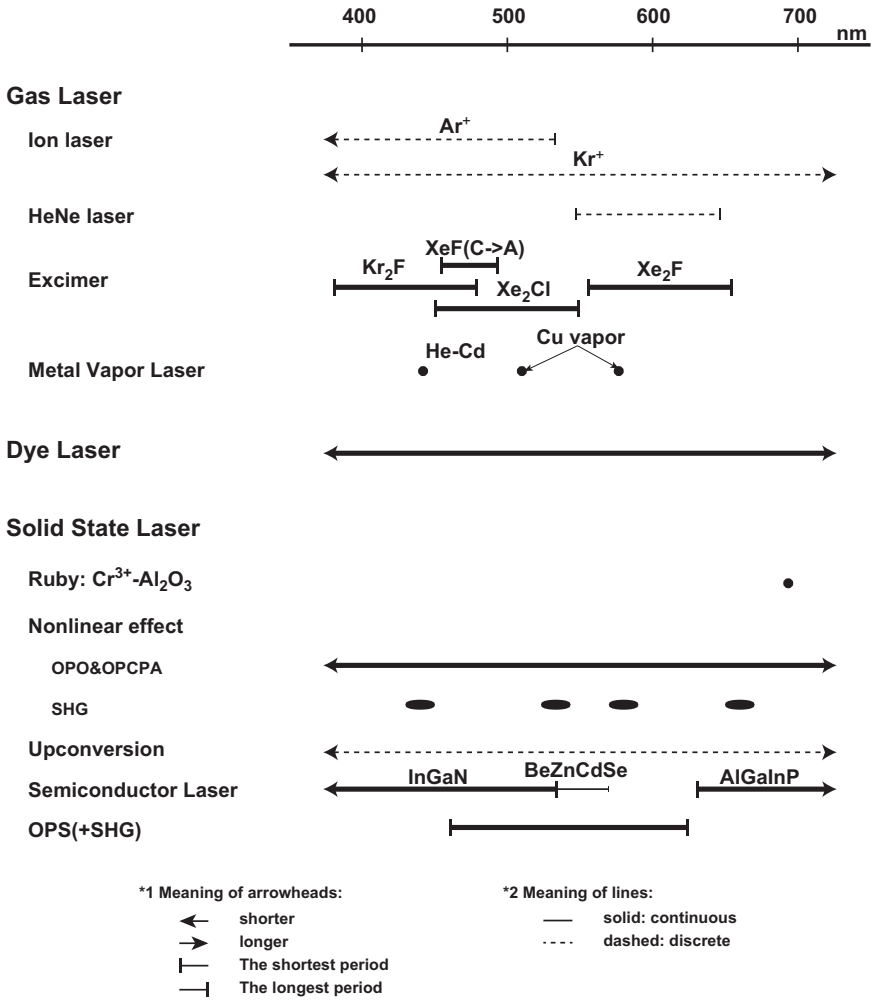

Fig. 2. Visible laser sources and their available wavelengths.

lasers with such attractive characteristics provide a different method than incoherent light for addressing the sun's mystery and encouraging research into solar power.

Next is a brief overview of previously developed visible laser systems. As mentioned above, visible light exists between 400 and 700 nm, and lasers are roughly classified into the following three categories: gas, liquid, and solid. To obtain visible coherent light, we utilize all phases of lasing case by case and sometimes use nonlinear optical effects in crystals. Several of best known visible laser sources and their available wavelengths are shown in Fig. 2.

The most prominent visible gas lasers are the rare-gas (Ar, Kr) ion lasers [5,6], HeNe lasers [7–9], excimer lasers [10–15], or metal vapor lasers [16–19]. These gas lasers are driven by a population inversion between energy levels of atoms or molecules in laser tubes by electrical discharge. In the gas phase, each transition between sublevels gives rise to discrete laser emission lines. On the other hand, it has been reported that excimer lasers show wideband and tunable properties, such as XeF ($C \rightarrow A$) (474 ± 20 nm) [12], Kr_2F (430 ± 50 nm) [13], Xe_2Cl (500 ± 50 nm) [14], and Xe_2F (605 ± 50 nm) [15]. Many metal elements have also been studied for metal vapor lasers, especially HeCd at 325 and 442 nm [16,17] and Cu at 511 and 578 nm [18,19]. The output power of copper vapor lasers is more powerful than that of other metal vapor lasers, and now output powers over 100 W have been achieved routinely [20,21].

Dye lasers, which are the only commercially available liquid laser, have been an important system for applications ranging from fundamental physics to clinical medicine for many years and continue because the distinctive feature of dyes as lasing media is their broad emission bandwidth (typically 50 nm) [22] with a tunable range, using appropriate dyes, between 300 and 1100 nm [23]. Continuous-wave (CW) and ultra-short pulse (femtosecond) operation [24] of dye lasers have been demonstrated, and high energy pulses around 400 J are also available [25]. Although the lifetime of the dye molecule upper loser level is very short on the order of ns [26,27], visible pulsed lasers such as a second harmonic of the Nd:YAG laser or a copper vapor laser are often used as excitation sources.

In order to realize visible solid-state lasers or coherent sources, the following have been proposed: nonlinear optical effects in crystals (second- or third-harmonic generation of an infrared laser, optical parametric oscillator (OPO)), upconversion phenomena in rare-earth doped materials, semiconductor lasers, and optically pumped semiconductor lasers (OPS). For example, for second-harmonic generation (SHG), two photons of a fundamental Nd:YAG laser at 1064 nm are converted into the second harmonic at 532 nm, in a nonlinear crystal. Since the wavelengths of fundamental lasers depend on active ions (Nd or Yb etc.), the specific transition of interest, and host materials, a certain spread is available in SHG wavelengths. On the other hand, wideband emission of OPOs has been reported as the third-order harmonic (355 nm), and the fourth-order harmonic (266 nm) of Q-switched Nd:YAG (1064 nm) can generate OPO ranges of 0.41–2.55 μm [28] and 0.33–1.37 μm [29], respectively. Such wideband emission is an appealing substitution for a dye laser; however, the system requires a pump of high peak power for nonlinear action and a higher photon energy of the pump than that for the signal wave. The upconversion phenomena in rare-earth doped materials [30,31] are also attractive for visible laser emission. Trivalent rare-earth ions are well suited for upconversion, especially Pr^{3+}, Nd^{3+}, Ho^{3+}, Er^{3+}, and Tm^{3+}. The unique feature of upconversion phenomena lies in the pumping process since lower energy photons are used for generating higher energy photon emissions; even infrared light can generate visible light. The other types of visible solid-state lasers are semiconductor lasers and optically pumped semiconductor lasers (OPS). The power of semiconductor lasers or OPSs continues to increase remarkably. These two lasers are very favorable for pump sources and will be introduced in the following section.

These visible lasers are already applicable in many technical areas, including display technology, medicine, laser processing, biology, metrology, and optical storage. For example, green laser sources are attractive for pointers and displays because green light is the most vivid color in the human photopic response, also known as the spectral luminous efficiency function. The color reproduction characteristics of laser displays are superior to liquid crystal displays in chromaticity diagrams [32]. Visible lasers are also used in photocoagulation surgery for diabetic retinopathy [33] because of the high absorbance of green light in melanin on retinal pigment epithelial cells [34], and minimal red light absorption by hemoglobin at bleeding sites [33]. Another aspect of a shorter wavelength laser is that the optical absorbance of a metal surface increases with shortening of the wavelength of light in most metals. Although copper absorbance is below 10% at 1 μm, it rises to 40% in the case of green light [35]. Since general laser processing uses a thermal process, a shorter wavelength laser is more effective than a longer one; visible lasers are also more effective than infrared lasers in laser processing.

When considering the importance of visible lasers, as explained at the beginning of this section, visible lasers have been developed using many pumping methods and with every material phase. Generally, a gas laser has good beam quality, but its system is large and inefficient. The SHG technique has the highest laser energy among current laser systems, such as the driver for inertial fusion driver [36], but it requires high fundamental wave peak power and generates discrete wavelength outputs. Dye lasers and OPOs show continuous, wideband spectra that are often applied to scientific research, but their systems have low efficiency with complicated system setups and operation. Semiconductor lasers are very useful for mass production, but the spectra range between 535 and 630 nm remains undeveloped, as we will show below. CW lasers emitting between 535 and 630 nm can also be realized by 2ω-OPS with compact structures.

In overviewing previous research on visible laser sources, such quality characteristics of photon beams as pulse duration, wavelength, and tunability have been considered more important than the photon beam quantity: in other words, photon beam cost. Specifically, little information concerning the cost of visible laser beams, relative to pick-up laser diodes for CD or DVD players, excitation laser diodes for Er-doped fiber amplifiers in optical communication networks, or high-power CO_2 lasers for laser processing. To expand the use of visible lasers in the future, design and development must concentrate on the quantity of photon beams on visible lasers while maintaining photon beam quality to broaden usage. Since high efficiency and system simplicity are required for such new lasers, one of the most promising considerations is a primary source, visible solid-state laser.

Next, we describe and discuss the primary sources of visible solid-state lasers, especially visible fiber lasers excited by GaN laser diodes.

2. Visible fiber lasers excited by GaN laser diodes

A primary source is a laser whose output photon energy is not determined by any nonlinear optical effect and, for an optically pumped laser is smaller than the excitation photon energy. Additionally, primary sources may be pumped by an electrical discharge in the gas phase. For example, an Nd:YAG laser excited by an 810-nm laser diode, a Yb-doped fiber laser excited by a 920-nm laser diode, and a Cu vapor laser are all primary sources of lasers. However, as we explained above, the development of primary sources in the visible region continues to fall well short of those in the infrared region, even though the first laser, the ruby laser, emits in the visible region. Thus, in the past visible, coherent sources have been derived from infrared laser sources

by nonlinear optical processes because of the following: (1) the stability, convenience, and compactness of the apparatus as compared with gas lasers and dye lasers; (2) the remarkable advances in infrared lasers, especially at the 1-μm region; and (3) the progress in the growth of nonlinear optical crystals such as BBO, LBO, cesium lithium borate (CLBO), KDP, and potassium titanyl phosphate (KTP) for second- or third-harmonic generation.

One crucial merit of visible primary sources is their efficiency. Even if we use the Yb-doped fiber laser one of the most efficient infrared lasers at 60–70% of optical–optical conversion efficiency to provide the fundamental , the efficiency of the SHG visible laser only reaches 35.4% using PPMgSLT [37]. On the other hand, as explained in the next section, a Pr^{3+} visible solid-state laser excited by GaN laser diodes exceeds 40% of optical–optical efficiency. Obviously, the emergence of an efficient primary source of a visible solid-state laser has been desired for a long time; however, it has not been successfully developed for the following reasons: (1) the lack of stable and cost effective excitation sources; and (2) the underdevelopment of solid-state laser media for efficient visible laser emission. The latter is the result of the development of infrared lasers, supported by the development of high-power semiconductor laser diodes for excitation sources and suitable solid-state laser host media.

In the following section, we consider activators and laser media for solid-state visible lasers and their history and present our waterproof fluoride glass fiber laser results to suggest the emergence of an efficient primary source of visible solid-state lasers, which we call a “primary visible solid-state laser.”

2.1. History of primary visible solid-state laser research

The history of primary visible solid-state laser research is summarized in Table 1. Recently, primary visible solid-state lasers have been actively developed by several research groups using fluoride host materials. Here, we review their history by focusing on rare-earth doped fluoride media, including glass fibers and crystals.

The first reported primary visible solid-state laser was the Pr:ZBLAN fiber laser, and a laser output of 250 mW at 635 nm was demonstrated by Smart et al. in 1991 [38]. One of the antecedents of primary visible solid-state laser research is upconversion laser research with Pr-doped fluoride fibers, and a report on upconversion visible lasers was also published by Smart et al. [39]. In 1994, a primary visible solid-state laser using Pr:YLF (praseodymium:yttrium lithium fluoride) was demonstrated by Sandrock et al. [40]. In 1995, Ruan et al. repored a mode-locked visible pulsed laser on Pr:YLF having a 90-mm-thick Schott Glass RG 610 filter as a saturable absorber. The visible pulse laser had a 8.5-ps pulse duration with 30-mW output power at 635 nm [41]. The following year, 400-fs pulse duration was demonstrated by the Kerr-lens mode-locking technique in Pr:YLF [42]. Thereafter, little research was done in this field for almost a decade because the demonstration phase was considered finished. Even though an Ar-ion laser system is large and expensive, researchers were compelled to use an Ar-ion laser for excitation in all of the above experiments, because it was the only available excitation source at that time. This means that this system was not practical for industrial use. On the other hand, infrared lasers such as the Yb-doped fiber and Nd:YAG lasers, have been widely developed due to the availability of high power semiconductor lasers; thus, the existence of effective excitation sources is essential for improving laser power and intensity. Because Er-doped fiber lasers or fiber amplifiers in optical communication also need single-mode operation as well as laser power, such excitation sources have been well developed. Once we obtain such effective excitation

Table 1
Historical study on primary visible solid-state laser research (focusing on rare-earth doped fluoride media including glasses and crystals).

Year	Host medium	Pumping source		Laser properties				Notes	Ref.
		Laser type	λ (nm)	λ_{em} (nm)	P_{out} (mW)	η_{slope} (%)	P_{th} (mW)		
Laser operation in Pr^{3+} doped fluoride materials									
1991	ZBLAN fiber	Ar-ion laser	476.5	491	6	2	150		[38]
				520	2	–	200		
				605	150	21.5	150		
				635	250	42	200		
				715	25	15	80		
1994	YLF	Ar-ion laser	457.9	522	144	14.5	163		[40]
				545	19	–	–		
				607	7	1.2	110		
				639.5	266	25.9	8		
				697	71	10.3	105		
				720	40	7.2	98		
				907.4	23	7.3	280		
1995	YLF	Ar-ion laser	476	607	110	8.5	400	Mode-locking:	[41]
				639	150	10	200	8.5 ps/30 mW/125 MHz at 639 nm, 10 ps/24 mW/100 MHz at 607 nm (90-mm-thick Schott Glass RG 610 filter used as a saturable absorber)	
1996	YLF	Ar-ion laser	476	613	45			Mode-locking: 400fs at 613 nm (0.98-nm FWHM)	[42]
2004	YLF	GaN laser diode	442	639.7	1.8	24	5.5		[45]
2005	ZBLAN fiber	2ω-OPS	479.7	635	94	41.5	50		[43]
2007	$LiLuF_4$	2ω-OPS	479.5	522.8	16	33	63		[49]
				607.2	34.5	31	26		

Table 1 (*continued*)

Year	Host medium	Pumping source		Laser properties				Notes	Ref.
		Laser type	λ (nm)	λ_{em} (nm)	P_{out} (mW)	η_{slope} (%)	P_{th} (mW)		
				640.2	52.7	56	10		
				721.5	50	46	12		
	YLF	2ω-OPS	479.5	523	600	46	159	Intracavity setup for generating SHG of 640 nm with a LBO crystal:	[44]
				607	350	32	105	364 mW in Pr:YLF	
				640	600	45	53	261 mW in Pr:LLF	
				720	570	43	52		
	$LiLuF_4$	2ω-OPS	479.5	523	470	53	201		
				607	370	35	77		
				640	570	52	66		
				720	500	56	99		
	YLF	GaN laser diode	444	640	61	28	75		
	$LiLuF_4$	GaN laser diode	444	640	76	36	59		
	KYF	GaN laser diode	446	644.5	39.4	23	125		[46]
2008	YLF	GaN laser diode	444	522	73	34	205		[47]
				607	42	14	105		
				640	185	41	42		
				720	129	30	157		
	$LiLuF_4$	GaN laser diode	444	607	36	12	122		
				640	208	38	111		
				720	149	24	133		
	$LiGdF_4$	GaN laser diode	444	522	18	28	288		
				607	56	20	128		
				640	174	53	139		
				720	105	33	82		
2009	WPFG fiber	GaN laser diode	442.6	448	0.7	–	104.3		[52]
				523	1.0	–	37		
				605	12.5	10	41.6		
				635	25.4	18.1	20.8		

	ZBLAN fiber	GaN laser diode	448	488 521 635 716 907	42 43 59 49 20	29 31 35 30 9	62 60 26 21 17	Tunable operation: 479–497 nm 515–548 nm 597–737 nm 849–960 nm	[50]
2010	WPFG fiber	GaN laser diode	442	638	311.4	41.6	52.1		[53]
2011	WPFG fiber	GaN laser diode	442	638	645.7	41.9	172.8		[54]
	YLF	GaN laser diode	443.9	522.6 545.9 607.2 639.5	773 384 418 938	61.5 52.1 32.0 63.6	148 728 125 30		[48]
	WPFG fiber	GaN laser diode	444	522.2	598	43.0	293.2		[55]
	ZBLAN fiber	GaN laser diode	442, 448	521	322	53	35		[51]
2012	WPFG fiber	GaN laser diode	444	523 638	950 1238	38.0 46.6	292 62	Overdrive operation 5 Hz/50% duty	Section 2.5.2
Laser operation in Dy^{3+} doped fluoride materials									
2000	ZBLAN fiber	Ar-ion laser	457	478 575	2.3 10	0.9 1.5	220 40		[65]
2010	WPFG fiber	GaN laser diode	398.8	575	10.3	17.1	10.2		[66]

OPS: Optically pumped semiconductor laser.
WPFG: waterproof fluoride glass (AlF_3 glass system).

sources for visible lasers at low cost, remarkable laser development progress is expected, as in the case for infrared lasers.

The next technological jump for primary visible solid-state laser development was initiated by new excitation sources, such as the 2ω-OPS and InGaN semiconductor lasers. In 2012, a 2ω-OPS system producing 7 W at 488 nm and a GaN laser diode of 1.6 W at 445 nm became commercially available. In 2005, a Pr-doped ZBLAN fiber laser excited by a 2ω-OPS was reported [43]. In 2007, 600 mW of output power at 640 nm in Pr:YLF was demonstrated [44]. GaN laser diode excitation has become the mainstream excitation source for Pr-doped laser media. The first demonstration of a Pr:YLF laser excited by a GaN laser diode was reported by Richter et al. in 2004 [45]. From 2007 to 2011, the output power improved to 39.4 mW at 644.5 nm [46], 208 mW at 640 mW [47], and to 938 mW at 639.5 nm [48]. A variety of host crystals was also tested, such as Pr:LLF [44,47,49], Pr:LGF [47], and Pr:KYF [46].

Even though the first primary visible solid-state laser with a fluoride medium was the Pr-doped ZBLAN fiber laser [38], no follow-up report on a primary visible fiber laser study appeared until 2005 [43]. In 2009, tunable laser operation of the Pr-doped ZBLAN fiber laser was demonstrated [50]. The tunable range (Table 1) widely covers the visible region because glass host media generally have a wide spectrum derived from inhomogeneous broadening, and therefore, visible fiber lasers are expected to be useful candidates for dye lasers. Finally, the maximum power of Pr-doped ZBLAN fiber lasers increased to 322 mW at 521 nm [51].

In 2009, a Pr-doped waterproof fluoride glass fiber laser was proposed and laser oscillation was demonstrated at four main Pr^{3+} emission wavelengths [52]. As described in Section 2.3, since the waterproof property of the AlF_3 glass system is far superior to that of ZBLAN glass, Pr-doped waterproof fluoride glass fiber is the most promising primary visible solid-state fiber laser medium. In 2010, its power increased to 311.4 mW at 638 nm [53] and in 2011 to 645.7 mW at 638 nm [54] and 598 mW at 522.2 nm [55].

In this paper, we mainly describe Pr-doped fluoride media lasers. However, the trivalent dysprosium ion (Dy^{3+}) is also a very attractive yellow source (575 nm) for visible solid-state lasers. Yellow lasers have been developed through several techniques, such as the copper bromide laser primary source [19], upconversion [56], or second-harmonic generation in Nd-doped crystals [57], Yb-doped fiber [58]. Also, a Bi-fiber laser [59], and optically pumped semiconductor lasers [60] are available because these lasers have many potential applications in biomedicine, ophthalmology, and medical treatment for acne melasma and facial telangiectasia [61]. Some materials doped with the Dy^{3+} ion after the possibility of laser oscillation [62–64]. However, laser oscillation was reported in only two papers [65,66]. Limpert et al. demonstrated yellow laser oscillation in Dy-doped ZBLAN fiber excited by an Ar-ion laser at 457 nm [65], and Fujimoto et al. reported a Dy-doped waterproof fluoride glass fiber excited by a GaN laser diode [66].

2.2. Activators for visible emission

Dieke et al. thoroughly researched the energy level diagrams of the rare-earth elements [67]. Many reports exist on visible emission from rare-earth ions, including Pr, Nd, Sm, Eu, Tb, Dy, Ho, Er, and Tm [31,68,69]. Some transition metals also emit visible light, but we mainly consider the rare-earth elements with visible emission, especially Pr^{3+} and Dy^{3+}. The energy level diagrams of Pr^{3+} and Dy^{3+} are shown in Fig. 3. The $^3P_0$ level in Pr^{3+} is the metastable state, and its lifetime is approximately several tens of μs and varies based on the host material. Although the most effective excitation line is the transition from $^3H_4$ to $^3P_0$ that corresponds to 482 nm, the transitions from $^3H_4$ to $^3P_{1,2}$, $^1I_6$ are also available because the $^3P_{1,2}$ and $^1I_6$ states are

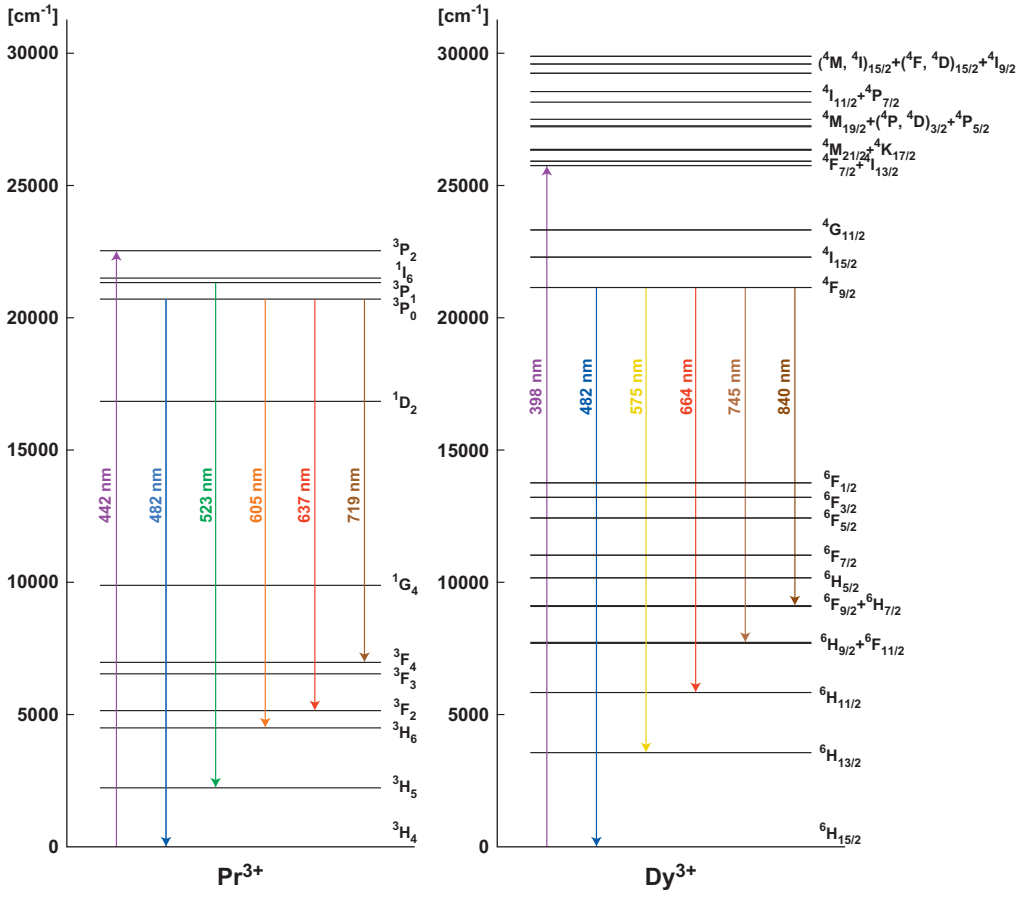

Fig. 3. Energy level diagrams of Pr^{3+} and Dy^{3+}.

rapidly thermally relaxed to the $^3P_0$ state. Similarly, the $^3P_0$ state decays to the lower energy levels based on their lifetimes with visible emissions that correspond to energy gaps between ionic excited states. There are five main emission lines: $^3P_0 \rightarrow {}^3H_4$ (482 nm); $^3P_1 \rightarrow {}^3H_5$ (523 nm); $^3P_0 \rightarrow {}^3H_6$ (605 nm); $^3P_0 \rightarrow {}^3F_2$ (637 nm); and $^3P_0 \rightarrow {}^3F_4$ (719 nm). Since the transition probability of $^3P_0 \rightarrow {}^3H_5$ is zero [70], thermally excitation of the $^3P_1$ state from the $^3P_0$ state becomes the initial state of 523-nm emission. Since the $^3P_0 \rightarrow {}^3H_6$ transition (605 nm) overlaps with the $^3H_4 \rightarrow {}^1D_2$ absorption line, the $^3P_0 \rightarrow {}^3F_2$ transition (637 nm) is the most common oscillation line of four-level systems in P^{3+}-doped materials.

On the other hand, Dy^{3+} is also an attractive source of yellow radiation. The $^4F_{9/2}$ state in Dy^{3+} is the metastable state, and its lifetime is around one ms and varies based on the host material. Although the most effective excitation line is the transition from $^6H_{15/2}$ to $^4F_{9/2}$ that corresponds to 482 nm, the other upper energy levels are also available for excitation through rapid relaxation to the $^4F_{9/2}$ state to produce florescence or losing a, for example, 398 nm. There are five main emission lines: $^4F_{9/2} \rightarrow {}^6H_{15/2}$ (482 nm); $^4F_{9/2} \rightarrow {}^6H_{13/2}$ (575 nm); $^4F_{9/2} \rightarrow {}^6H_{11/2}$ (664 nm); $^4F_{9/2} \rightarrow {}^6H_{9/2}+{}^6F_{11/2}$ (745 nm); and $^4F_{9/2} \rightarrow {}^6F_{9/2}+{}^6H_{7/2}$ (840 nm). The yellow emission

line of $^4F_{9/2} \rightarrow {}^6H_{13/2}$ in Dy^{3+} is very impressive because effective yellow emission is rare in solid-state laser materials.

2.3. Host materials

2.3.1. Fluoride materials

As explained in Section 2.2, many rare-earth elements have the possibility for visible emission. However, rare-earth elements have many energy levels and some combinations of emissive rare-earth elements and host materials relax the populations at the metastable state through a multi-phonon relaxation process. Since the possibility of a multi-phonon relaxation process is related with the maximum phonon energy in the host material and oxide materials have relatively high phonon energy, emissive rare-earth elements in oxide hosts are limited [71].

The advantage of fluoride materials has been frequently discussed. The most important characteristic is that their phonon energies are lower than those for the oxide materials. Indeed, the phonon energy of fluoride glass is one-third or half that of oxide glass [71]. There are other glass systems suitable for visible emission; for example, chloride glass has phonon energies less than that of fluoride [71] and tellurite glass in which visible emissions were reported [72]. However, fluoride laser materials are most actively developed as low phonon energy laser host materials. The properties of the available fluoride glass systems are summarized in Table 2.

Glasses based on beryllium fluoride (BeF_2) were first identified by Goldschmidt in 1926 [73]. Fluoride glass is a relatively new material, since less than a hundred years has passed since its discovery, as contrasted with oxide glass's 4000 year history. BeF_2, which is the only material vitrified by a single component, forms a four-coordination state like silica glass. After this discovery, many researchers explored its applications. BeF_2 was proposed as a high-power Nd-doped laser host material for a fusion driver because of its low nonlinear refractive index coefficient [74,75]. However, the toxicity of BeF_2 compounds and high water solubility were apparent [76], and now a BeF_2 glass system is considered unsuitable for commercial use.

Table 2
Properties of available fluoride glass systems.

Glass system	Components	Notes
BeF_2	BeF_2	High hygroscopicity, toxicity ZBLAN fiber commercially available
ZrF_4	$ZrF_4 \cdot BaF_2 \cdot LaF_3 \cdot AlF_3 \cdot NaF$ (ZBLAN)	High hygroscopicity Low glass transition temperature (250–300 °C) Low-loss optical fiber (0.1 dB/m) available Waterproof property
AlF_3	$AlF_3 \cdot YF_3 \cdot CaF_2 \cdot BaF_2$	High glass transition temperature (350–430 °C) Easy crystallization in comparison with ZBLAN Y is an expensive rare metal element.
ThF_4	$ThF_4 \cdot BaF_2 \cdot LiF$	Th is a radioactive element.
GaF_3	$GaF_3 \cdot PbF_2 \cdot ZnF_2$	Ga is an expensive rare metal element.
InF_3	$InF_3 \cdot BaF_2 \cdot YF_3$	Good infrared transparency (suitable for optical fiber amplifier at 1.3 μm) In and Y are expensive rare metal elements.
ZnF_2	$ZnF_2 \cdot BaF_2 \cdot YF_3$	Easy crystallization compared with ZBLAN
CdF_2	$CdF_2 \cdot BaF_2$	Cd is a pollution element.

The next discovery of a fluoride glass material was ZrF_4–BaF_2–NaF glass by Poulain et al. [77]. The ZrF_4–BaF_2–NaF glass system became the most common fluoride glass of the ZrF_4–BaF_2–LaF_3–AlF_3–NaF glass system (ZBLAN); however, ZBLAN glass also exhibits high water solubility [78]. From the viewpoint of seeking a insoluble fluoride glass, AlF_3 system glass was actively researched [78,79]. In 1991, Iqbal et al. demonstrated its waterproof property by comparing its weight loss in water to ZBLAN glass. The weight loss of ZBLAN glass in water at 23 °C for 24 h reached 5.23 wt%, but the weight loss of AlF_3 system glass was only 0.01 wt%. This result conclusively demonstrated the waterproof property of AlF_3 system glass.

Optical fiber research using fluoride glass began in 1980, and results were reported by the NTT group (GdF_3–BaF_2–ZrF_4 glass) [80], the Rutgers University group (AlF_3 glass system) [81], and Szebesta et al. [82]. The 1.3-μm wavelength corresponds to the zero dispersion wavelength of single mode optical silica fibers [83], which are often used in metro optical communication networks. A Pr-doped ZBLAN fiber for an optical amplifier at 1.3 μm has been actively developed and commercialized by FiberLabs Inc.

2.3.2. *Waterproof fluoride glass and fiber*

Our group has been developing AlF_3 system fluoride glass and fiber without alkali metals [79] because of the glass system's excellent waterproof property, even though it is fluoride glass. We call our AlF_3 system waterproof fluoride glass (WPFG). To examine its durability in high humidity conditions, we carried out the following test with two Pr:WPFG test samples whose Pr concentration was 2000 ppm and whose size was 10∗10∗1 mm^3. The first sample was put in air at room temperature (usual room condition). The second sample was put in an oven at 80 °C with humidified air that was prepared using a wrapped double cup (Fig. 4), which was constructed as follows. The outer cup was filled with water, and a test-bulk sample was put in the inner cup. The double cup was then wrapped in aluminum foil. The endurance test continued for 36 days. Photographs and the measured weights of the samples of the endurance test are shown in Fig. 5. The first sample in air at room temperature did not show any change in appearance or transmittance spectrum even after 36 days. The second sample under the highly humidified condition also did not show any change in appearance; however, the transmittance slightly decreased in the violet region by 2% or 3% (Fig. 6), and its weight increased by 0.01 g after the endurance test, but there was no weight change in the first sample. Therefore, moisture might seep into the sample and cause scattering or absorption in the sample or on the surface. This simple endurance test reveals that WPFG has enough durability against humidity if we use it

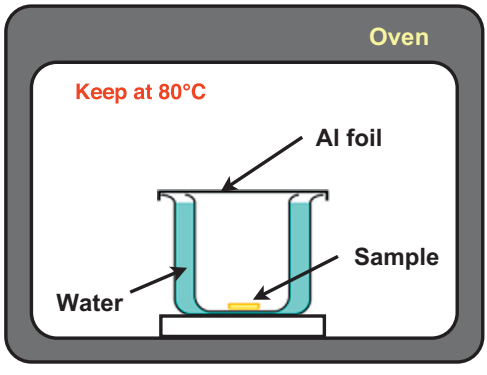

Fig. 4. Setup of endurance test of AlF_3 system fluoride glass in an oven at 80 °C.

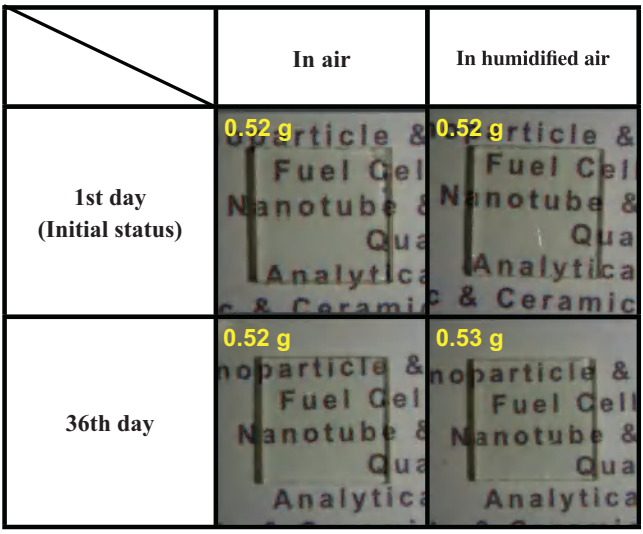

Fig. 5. Progress photographs of endurance test before and after 36 days.

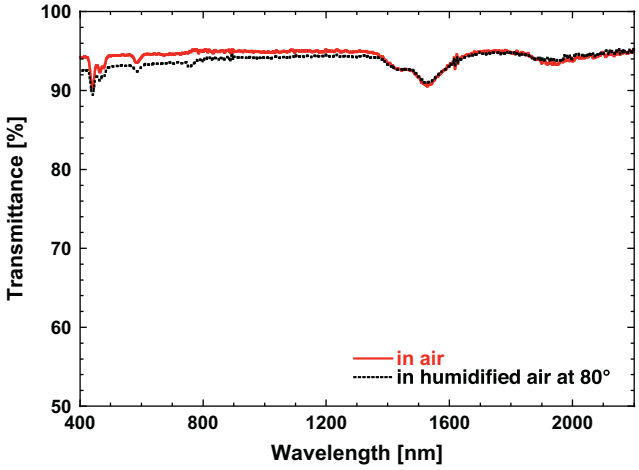

Fig. 6. Transmittance spectra of samples in air and in humidified air at 80 °C after endurance test.

under usual room conditions. This is also supported by the stable laser operation of this WPFG fiber with adequate laser power reproducibility over a period of one or more years.

Based on the above results, since AlF_3 system fluoride glass is very interesting as a laser active medium, especially for fiber lasers, many researches have tried to fabricate them. Iqbal et al. reported that the optical loss in AlF_3 system fluoride glass was 7.5 dB/m [78], because it can easily be crystallized, and microcrystals in the glass can cause larger scattering loss. Since a large loss would obviously prevent efficient fiber laser operation, our group has been developing a low-loss AlF_3 system fluoride glass optical fiber. In 2009, Ishii and Yamazaki decreased the loss

of AlF_3 system fluoride glass optical fiber to 0.1 dB/m [52], the same loss value as commercial ZBLAN fiber. This value is adequate for mimizing the power loss in a fiber laser.

2.4. Excitation sources

Since the present progress of solid-state lasers greatly reflects the development of excitation sources, the development of such excitation sources as laser diodes has contributed greatly to improving the laser power and intensity as well as the beam quality of solid-state lasers such as Er-doped fiber lasers, Yb-doped fiber lasers, and Nd:YAG lasers. The same statement is also true about visible solid-state laser development. Once we can obtain such effective excitation sources for visible lasers at low cost, remarkable visible laser development is expected as was the case with infrared lasers. Next we review the excitation sources used for Pr-doped fluoride crystal and fluoride glass fiber lasers.

2.4.1. Ar-ion lasers

First, we consider Ar-ion lasers. From an historical perspective, Ar-ion lasers were used as a pump source at an early stage. Argon's energy level diagram is shown in Fig. 7 [5]. The energy needed to ionize argon is about 16 eV, and an additional 20 eV is required to reach the states that decay to the upper laser level. The upper and lower laser levels that generate visible emission are the 4p and 4s states. The energy gap between 4p and 4s is about 2 eV. In comparing this total energy input of 36 eV to the energy emitted by the laser transition itself (2 eV), the efficiency of an argon ion laser is clearly very low. The 4p and 4s energy states are separated into several sublevels, and each transition between sublevels gives rise to discrete laser emission lines between 454.4 and 524.5 nm. The most powerful emission line is the 4p ($^4D_{5/2}$) to 4s ($^2P_{3/2}$) transition at 514.5 nm, and 20 W systems have been commercially available for decades. The 476.5- and 457.9-nm lines of an Ar-ion laser are often selected for the excitation lines of the Pr-doped fluoride materials (Table 1).

2.4.2. Optically pumped semiconductor lasers (OPSs)

OPSs, which are also known as vertical external-cavity surface-emitting lasers (VECSELs) [84], have a gain medium layer stacked on a semiconductor mirror layer set inside a bulk optics

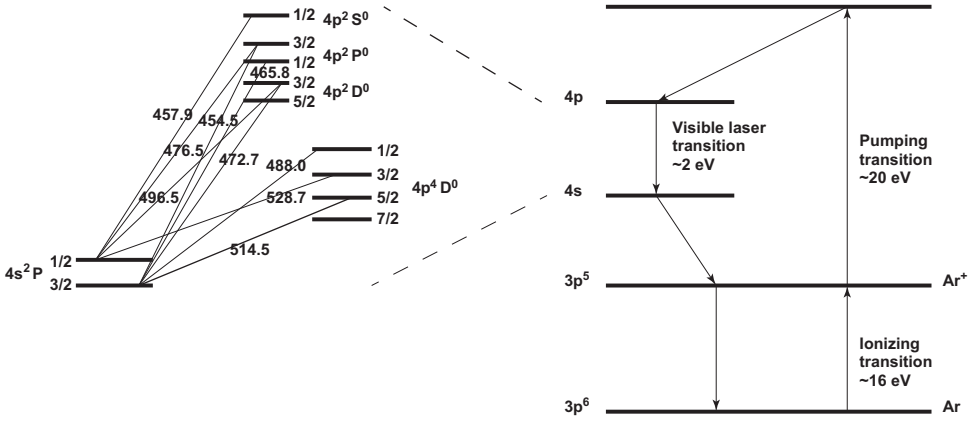

Fig. 7. Energy level diagram of argon.

cavity. The gain medium is optically pumped by an external laser source, which is often a semiconductor laser. Since the spectral bandwidth of the semiconductor gain media is between 920 and 1250 nm, if we put a nonlinear crystal for SHG in the cavity, wideband visible emission between 460 and 625 nm is produced with such an intra-cavity setup.

The power available from frequency-doubled OPS (2ω-OPS) systems has been increased dramatically so as to be suitable for many applications. For example, 7 W at 460 nm [85], 15 W at 488 nm [86], 5 W at 589 nm [60], and 2.7 W at 612 nm [87] have been achieved. Although 2ω-OPS visible lasers use the SHG technique, they are often used as a convenient coherent light source because they are compact, and offer adequate optical–optical efficiency (20–30%). The 479.5-nm emission from one 2ω-OPS system was selected as the excitation for Pr-doped fluoride materials (Table 1). As another possible of visible OPS research using GaN wafers has already started, and it is likely that such devices will be developed in the near future [88].

2.4.3. *Visible semiconductor lasers*

Two types of semiconductor systems, AlGaInP and InGaN, are commonly used to fabricate visible semiconductor lasers. A semiconductor of an AlGaInP system typically emits in the red region [89]. Yellow emission from an AlGaInP system semiconductor laser was demonstrated at liquid nitrogen temperature [90,91]; however, a shorter wavelength has not been reported.

Semiconductor lasers emitting at wavelengths below 600 nm have been researched for many years with ZnSe and ZnS systems [89]. In 1994, a blue light-emitting diode of an InGaN system was discovered by Nakamura et al. [92], and after that, it became blue semiconductor laser material of choice. The power of InGaN laser diodes has increased to 1.6 W at 445 nm. This intense blue emission from an InGaN laser diode is commonly chosen for the excitation of Pr-doped fluoride materials (Table 1). The next target is a green and yellow semiconductor laser with wavelengths between 500 and 600 nm, and many researchers are concentrating on developing them. For example, 70 mW of pulsed operation laser power at 500 nm [93] and 60-mW-CW at 521 nm [94] have been reported for InGaN systems. The longest laser wavelength

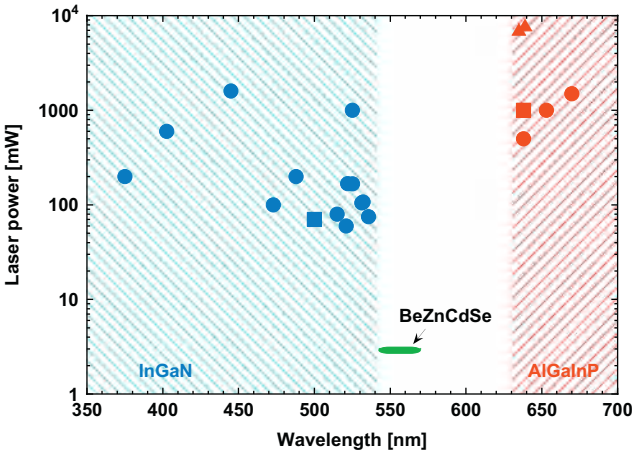

Fig. 8. Semiconductor laser powers operated at room temperature in visible region. Circles are CW lasers, squares are pulse lasers, and triangles are arrayed-CW lasers. Data are adopted from Refs. [93–96] and laser diodes catalogs of Nichia Corporation, Mitsubishi Electric Corporation, Sony Corporation, and eagleyard Photonics GmbH in 2012.

with InGaN systems is at 535.7 nm and the maximum power generated to date is 75 mW [95]. In 2012, the Nichia Corporation announced on their homepage a high-power green laser diode, operating at 525 nm and producing 1 W. Regarding other semiconductor systems, laser oscillation of 3.0 mW was demonstrated between 543 and 570 nm in the BeZnCdSe system [96].

The output powers currently available from semiconductor lasers, operating in the visible at room temperature, are summarized in Fig. 8. Clearly there are not enough semiconductor lasers of sufficient power between 535 and 630 nm. For the application of a laser TV, a green laser producing over 10 W can be obtained using the SHG technique by combining Nd:YVO_4 with a PPMgLN nonlinear crystal [32]. Further investigation of semiconductor lasers and increases of the laser power in this wavelength region will easily provide more vivid color reproducibility in display systems than commonly used liquid crystal displays.

In general, semiconductor lasers have high efficiency because their drive current is readily converted to optical power. On the other hand, the beam patterns are not good because semiconductor lasers are typically designed as an array structure to obtain higher power. Single-mode semiconductor lasers are commercially available, but maximum power is limited to several hundred mW for the most powerful infrared devices. Therefore, a high-power single mode semiconductor laser is highly desirable an optical pump in its own right.

2.5. *Waterproof fluoride glass (WPFG) fiber laser*

2.5.1. *Spectroscopic properties*

2.5.1.1. Pr:WPFG. The absorption and fluorescence spectra of Pr:WPFG are shown in Fig. 9. The Pr concentration is 3000 ppm. There are four absorption peaks: 444, 468, 480, and 590 nm. As mentioned above, the absorbed light at 444, 468, and 480 nm results in the transfer of energy to the $^3P_0$ meta-stable level in Pr^{3+} and is stored during its lifetime. On the other hand, the absorbed light at 590 nm does not contribute to any visible emissions.

As shown in Fig. 3, there are mainly five emission lines in the visible region. The emissive transitions of $^3P_1 \rightarrow {}^3H_5$ and $^3P_0 \rightarrow {}^3H_6$, $^3F_2$, $^3F_4$ work as four-level systems. Only the transition of $^3P_0 \rightarrow {}^3H_4$ (482 nm: the first peak) is a three-level system and overlaps the $^3H_4 \rightarrow {}^3P_0$ absorption line. The transition of $^3P_0 \rightarrow {}^3H_6$ (605 nm) also overlaps the absorption line of $^3H_4 \rightarrow {}^1D_2$. Therefore, the threshold powers become higher, and their efficiencies are expected to be lower

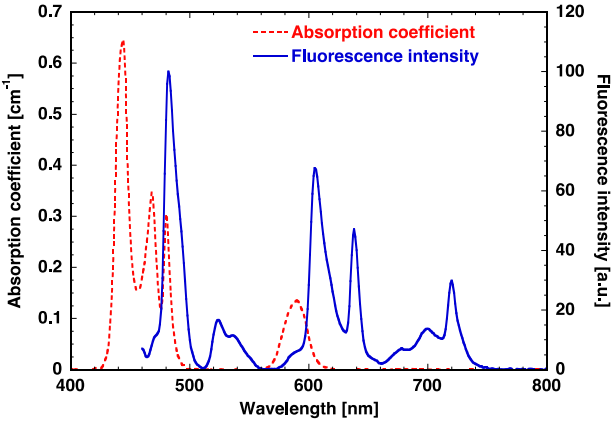

Fig. 9. Absorption and fluorescence spectra of Pr:WPFG. Pr concentration was 3000 ppm.

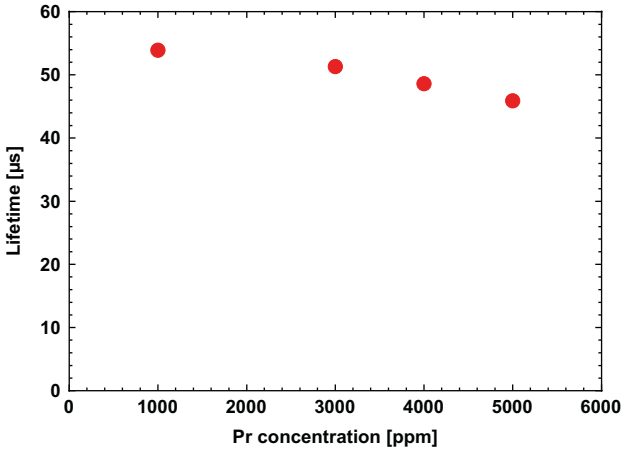

Fig. 10. Dependence of lifetime on Pr concentration of Pr:WPFG.

for laser operations at 482 and 605 nm. Even though the $^3P_1 \rightarrow {}^3H_5$ (523 nm) transition is a four-level system, the height of the fluorescence peak is about one-third of the $^3P_0 \rightarrow {}^3F_2$ (637 nm) peak, and the gain at 523 nm is expected to be lower than that at 637 nm. Therefore, the most common transition is $^3P_0 \rightarrow {}^3F_2$ (637 nm), even if it is the third peak in Pr:WPFG.

The absorption and fluorescence spectra of Pr:WPFG are very broad compared with the crystal spectra [45,47,49] due to the inhomogeneous crystal field in the glass. There is concern that this phenomenon might reduce the stimulated emission cross section which is proportional to the gain coefficient. Thus, the gain coefficient is expected to be lower than that for the crystal materials. However, an optical fiber is drawn from a glass medium and the gain length can be optimized. Indeed, a wide fluorescence spectrum is critical in tunable and ultra-fast operation, and a tunable laser was already reported with Pr:ZBLAN fiber [50].

The dependence of the lifetime on the Pr concentration in Pr:WPFG is shown in Fig. 10. The fluorescence for the lifetime measurement was detected at 635 nm. Pr:WPFG's lifetime at 3000 ppm was measured to be 51.3 μs, and strong concentration quenching was not observed up to Pr concentration of 5000 ppm.

2.5.1.2. Dy:WPFG. The absorption and fluorescence spectra of Dy:WPFG are shown in Fig. 11. The Dy concentration was 10,000 ppm. Absorption peaks exist at 389, 427, 453, and 473 nm. The absorbed light at 389, 427, and 453 nm is transferred to the $^4F_{9/2}$ meta-stable energy level in Dy^{3+} and stored in this level during its lifetime.

As shown in Fig. 3, there are mainly three visible emission lines. Only the $^4F_{9/2} \rightarrow {}^6H_{15/2}$ transition works as a three-level system, whereas the other emissive transitions, $^4F_{9/2} \rightarrow {}^6H_{13/2,11/2}$, $^6H_{9/2}+{}^6F_{11/2}$, and $^6F_{9/2}+{}^6H_{7/2}$, are work as four-level systems. The most common transition is $^4F_{9/2} \rightarrow {}^6H_{13/2}$ which lies in the yellow (575 nm). Yellow laser oscillation—that is, the realization of a solid-state primary source has been difficult to obtain in the past, and the copper vapor laser is the only commercially available primary yellow laser. The transition of $^4F_{9/2} \rightarrow {}^6H_{15/2}$ (482 nm) is also an important laser line, but it overlaps the absorption line of $^6H_{15/2} \rightarrow {}^4F_{9/2}$. The transition of $^4F_{9/2} \rightarrow {}^6H_{9/2}+{}^6F_{11/2}$ (664 nm) is also a four-level system; however, the height of the fluorescence peak is about one-tenth that of the $^4F_{9/2} \rightarrow {}^6H_{13/2}$ transition (575 nm); therefore

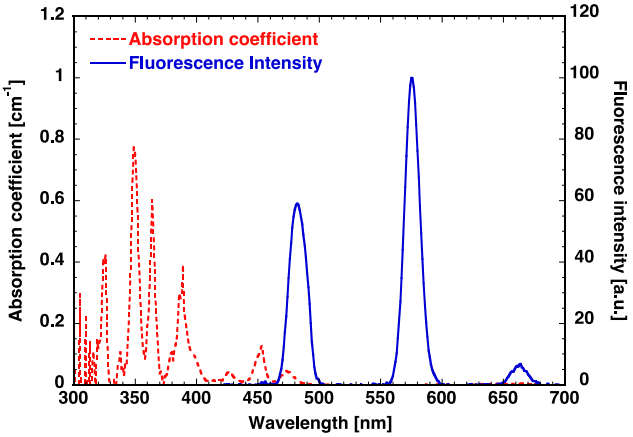

Fig. 11. Absorption and fluorescence spectra of Dy:WPFG. Dy concentration was 10,000 ppm.

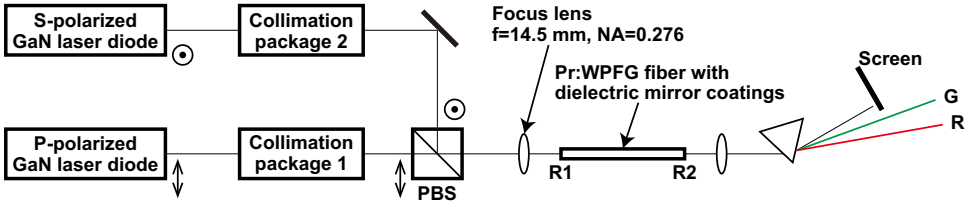

Fig. 12. Setup of laser oscillation experiment for Pr:WPFG fiber.

the gain at 664 nm is expected to be much lower than that for the yellow line. The lifetime for the $^4F_{9/2}$ state was measured to be 1.03 ms at 575-nm emission with 389-nm excitation. The fluorescence spectrum of Dy:WPFG is also wide. Therefore, this material is also expected to be well-suited for tunable and ultra-fast lasers.

2.5.2. *Laser operation*

In a report published in 2009, we demonstrated a multi-wavelength fiber laser with Pr-doped waterproof fluoro-aluminate glass (Pr:WPFG) excited by a GaN laser diode [52]. In 2010, the laser power at 638 nm from a Pr:WPFG fiber increased to 311.4 mW with a slope efficiency of 41.6% [53].

To produce a more powerful visible fiber laser (for example, over 1 W), several techniques can be applied to increase the brightness of the excitation power. One is to have a more powerful excitation source of GaN laser diodes. The other is to bundle several excitation sources. We considered three bundle methods: counter-excitation, polarization combining, and power combining with bundled fibers. Power fiber-combines with bundled fibers are usually used in high-power Yb-doped fiber lasers; however, such devices for GaN laser diodes remain inadequately developed. Generally, an edge-emitting laser diode is polarized to the slow axis because the polarization of heavy hole emissions in semiconductors is dominated by the waveguide's transverse electric (TE) mode [89]. Therefore, the power of edge-emitting laser diodes can be bundled by a properly designed polarization combining setup.

2.5.2.1. Pr:WPFG fiber laser. The setup for our laser oscillation experiment for a Pr:WPFG fiber is illustrated in Fig. 12. Two GaN laser diodes (Nichia Corporation: NDB7352E) were used as excitation sources. Each collimation package includes a collimation lens ($f=8.0$ mm, NA$=0.5$) and an anamorphic prism pair with a magnification of 4. The slow axis of the GaN laser diode was set to the magnifying axis in the anamorphic prism pair. The two GaN laser diode beams in Fig. 12 were P- and S-polarized because the GaN laser diode is polarized to the slow axis [89]. The two beams were combined in a polarizing beam splitter (PBS) to one beam line and focused onto a Pr:WPFG fiber input surface by a 14.5-mm focusing lens having a numerical aperture (NA) of 0.276. The residual excitation beam from the Pr:WPFG fiber was separated by a prism and cut by a screen.

Both GaN laser diodes were operated at the rated operating current (1200 mA). The maximum output powers of the P- and S-polarized GaN laser diodes were 971 and 1364 mW. The difference of the maximum output powers was considered as individual difference. The polarization ratio to the slow axis of both GaN laser diodes was measured to be around 90%. The loss of the PBS was 9.8%, and we roughly estimated that over 80% of the power of the two GaN laser diodes can proceed by combining the two in PBS.

A Pr:WPFG fiber with dielectric multilayered coatings provided the laser cavity. The Pr concentration was 3000 ppm. A Pr:WPFG fiber was fastened to a zirconia ferrule (Fig. 13), and Pr:WPFG fiber with a zirconia ferrule is now commercially available from Sumita Optical Glass, Inc. The core/clad diameters were 16/300 μm, and the fiber length was 40 mm. The GaN laser diode peaks were at 444 nm, and the absorption coefficient of the Pr:WPFG fiber was 0.56 cm^{-1}; therefore, about 89.4% of the GaN laser diode light was absorbed by the fiber. The NA of the Pr:WPFG fiber was 0.235 at 444 nm.

2.5.2.1.1. Green laser. Dielectric multilayered coatings were deposited on both end surfaces of the Pr:WPFG fiber as resonator mirrors. The reflectivities at 719, 638, 605, and 522 nm and the transmittance at 444 nm of the R1 surface (Fig. 12) were 20.6%, 69.4%, 94.0%, 99.95%, and 99.0%, respectively. For selective oscillation at 522 nm, the reflectivities at 719, 638, 605, and 522 nm of the R2 surface (Fig. 12) were 6.0%, 4.6%, 0.7%, and 94.9%, respectively.

The input–output characteristics plot for the Pr:WPFG fiber laser in the CW mode is shown in Fig. 14. The horizontal and vertical axes show the absorbed power in the Pr:WPFG fiber and the output power at 522.2 nm. The threshold power was measured to be 293.2 mW, and maximum output power obtained was 598 mW at an absorbed power of 1695 mW. The slope efficiency was 43.0%.

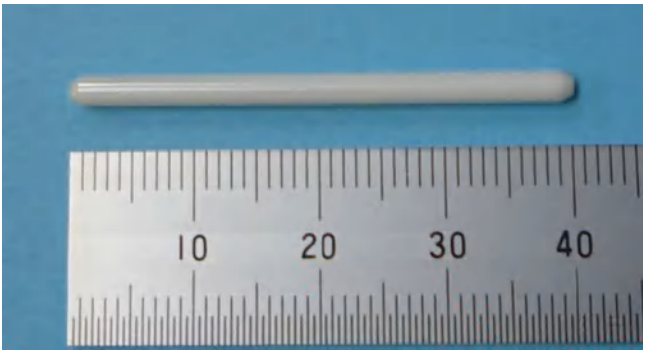

Fig. 13. Pr:WPFG or Dy:WPFG fiber with zirconia ferrule (40 mm). Pr:WPFG fiber with a zirconia ferrule is now commercially available from Sumita Optical Glass, Inc.

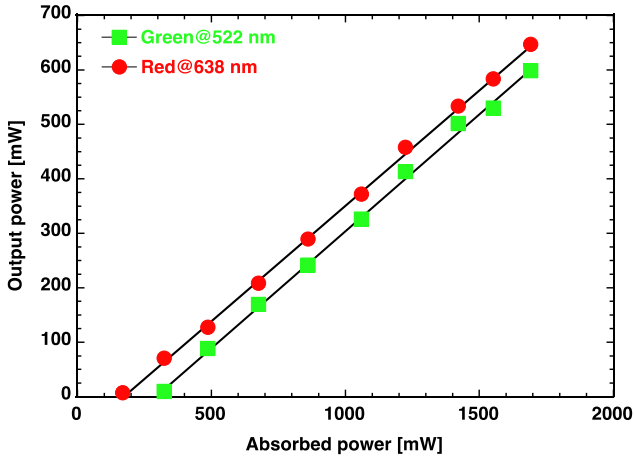

Fig. 14. Input–output characteristics plot of Pr:WPFG fiber laser in CW mode.

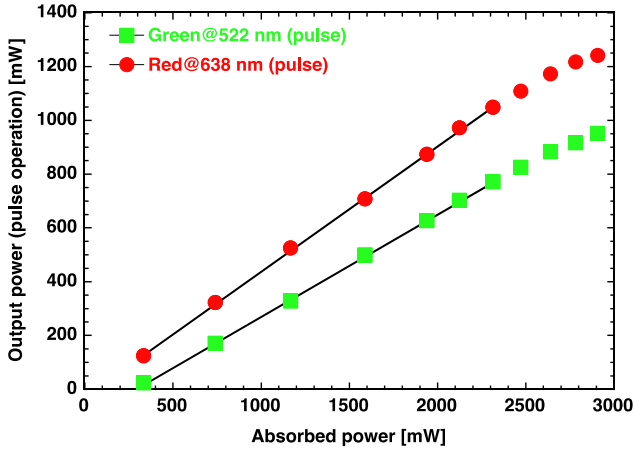

Fig. 15. Input–output characteristics plot of Pr:WPFG fiber laser in overdrive pulse mode. Two GaN laser diodes of 1200 mA rated current were operated under maximum peak current of 1800 mA at 5 Hz with 50% duty (100-ms on/off).

Since the thermal conductivity of the GaN semiconductor is comparatively higher than other semiconductor materials [97], a GaN laser diode can work over the rated peak output power in pulsed operation. Such an experimental setup was identical to that of Fig. 12, but two GaN laser diodes of 1 W rating were operated at a maximum peak power of 1.8 W at 5 Hz with 50% duty (100 ms on/off). We refer to this operation mode the overdrive pulse mode. The pulse peak output of the green laser is plotted in Fig. 15. Maximum peak power obtained was 950 mW with 292 mW of threshold power pump power and a slope efficiency of 38.0%.

The pulse output did not increase linearly during high-power pumping (Fig. 15). This phenomenon depends primarily on the characteristics of the GaN laser diodes excitation. Because the temperature of the GaN laser diode chip increased with rising laser diode power, even though the temperature of the GaN laser diode package was controlled at 25 °C, we operated at a peak current of 1800 mA with 50% duty quasi-CW mode operation in an overdrive

pulse mode for the rated current 1200 mA to the GaN laser diodes. The following phenomena appeared due to the temperature increase and the overload current: (1) the decrement of absorption power caused by the peak wavelength shift with increasing temperature of the GaN laser diode chip; (2) the optical coupling mis-match between the actual focusing NA and the Pr:WPFG fiber NA, which was caused by the change in divergence of the emitting light. For the first case, when we used a GaN laser diode operating initially at 442 nm, the wavelength moved to 446 nm at 1800 mA of operating current. However, the absorption band of Pr:WPFG at 442 nm sufficiently broad to compensate for the wavelength shift, and the loss in absorption power is estimated to be only 2% at maximum. In our tests, the second case of optical mismatched coupling was more problematic. When we used a GaN laser diode at 1800 mA of operating current, the emitting light's divergence increased, and the actual focusing NA also increased. The NA mismatch of the slow axis was greater than that for the fast axis because the slow axis was magnified by an anamorphic prism pair with a magnification of 4. For example, the slow axis NA of a GaN laser diode (Nichia Corporation: NDB7875, 1.6 W) was measured to be 0.147 but this value increased with rising laser diode power, eventually reaching 0.268 when the diode was operated over the rated current. Since the NA of the Pr:WPFG fiber in Fig. 12 was 0.235, the loss of coupling efficiency reached 13%, provided that the slow axis NA characteristics of the GaN laser diodes (NDB7352E) are the same as those tested (NDB7875). Based on the above estimate, when we use the overdrive pulse mode in the GaN laser diode for laser excitation, we must be concerned about the change in divergence of the emitting light with current by optimally designing an excitation optical system.

2.5.2.1.2. Red laser. Dielectric multilayered coatings were deposited on both end surfaces of the Pr:WPFG fiber as resonator mirrors. The reflectivity at 638 nm and the transmittance at 444 nm of the R1 surface (Fig. 12) were 99.96% and 97.9%, respectively. For selective oscillation at 638 nm, the reflectivity at 638 and 605 nm of the R2 surface (Fig. 12) was 80.8% and 63.9%, respectively.

The input–output characteristics plot of the Pr:WPFG fiber laser is shown in Fig. 14. The horizontal and vertical axes show the absorbed power in the Pr:WPFG fiber and the output power was 638 nm. The threshold power was measured to be 172.7 mW, and maximum output power obtained was 646 mW for an excitation power of 1695 mW. The slope efficiency was calculated to be 42.4%.

The overdrive pulse mode was also tested for the red laser. The experimental setup and parameters were the same as the CW-operation above except that the core diameter of the Pr:WPFG fiber was 14 μm. The instantaneous peak output of the red laser is also plotted in Fig. 15. The maximum peak power was 1238 mW with 62 mW of threshold power and 46.6% of slope efficiency. The reason for the nonlinearity at high-power pumping is presumed to be the same as for the green laser. A photograph of the red laser oscillation in operation is shown in Fig. 16.

2.5.2.2. Dy:WPFG fiber laser (yellow laser). Fluoro-aluminate glass including a Dy concentration of 10,000 ppm of Dy concentration was used in the fiber core. The core and cladding diameters of the drawn fiber were 8 and 300 μm, respectively. The fiber's NA was 0.23. A 40-mm-long Dy:WPFG fiber was inserted into a zirconia ferrule (as in Fig. 13), and both ends of the fiber were polished.

The setup of the laser oscillation experiment is illustrated in Fig. 17. A violet GaN laser diode at 398.8 nm (Nichia Corporation: NDV7112) was used as the excitation source. The absorption peak at 398.8 nm was measured to be 0.091 cm^{-1}. Thus, for example, if we used the 40-mm-long Dy:WPFG fiber, 30.5% of the excitation source power at 398.8 nm will be absorbed. The emitter

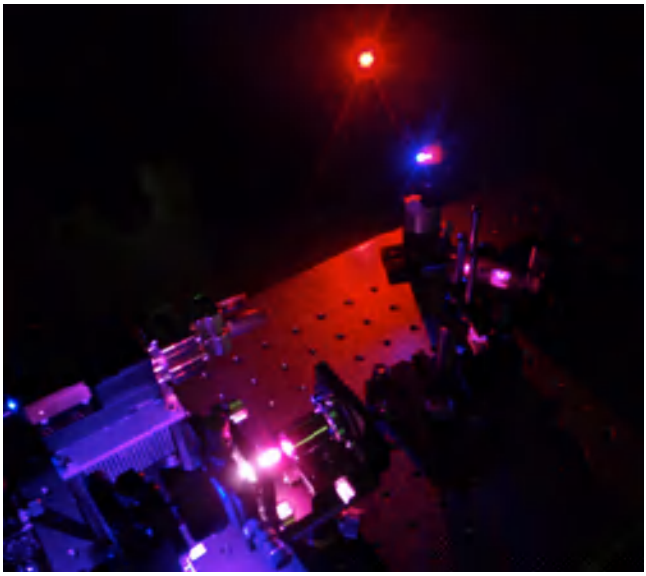

Fig. 16. Photograph of red laser oscillation.

size of the GaN laser diode was 7 μm. The violet laser diode beam was collimated by a lens with a focal length of 8 mm and an NA of 0.5, and the collimated laser diode beam was shaped into a quasi-disc by an anamorphic prism pair. Next, the laser diode beam was focused into the Dy:WPFG fiber by a 14.5-mm focusing lens having an NA of 0.276. Commercial dielectric filters were used as the cavity mirrors for R1 (rear mirror) and R2 (output mirror), and the mirrors were in close contact with both fiber end surfaces. The reflectivity at 575 nm of the R1 and R2 mirrors was 99.9% and 93.3%, respectively. The transmittance at 398.8 nm of R1 and R2 was 96.5% and 94.6%, respectively. Since the reflectivity at 398.8 nm of the R1 mirror was 3.5%, the excitation source was effectively delivered to the Dy:WPFG fiber. On the other hand, since the reflectivity at 398.8 nm of the R2 mirror was 5.4%, a remarkable portion of the excitation power was emitted from the Dy:WPFG fiber because, as estimated above, only 30% of the excitation source power at 398.8 nm can be absorbed by the 40-mm-long Dy:WPFG fiber. The output beam was divided into yellow and violet beams by a dichroic mirror. The absorbed pump power into the Dy:WPFG fiber was directly measured by subtracting the power exiting the Dy:WPFG fiber from the power entering the Dy:WPFG fiber (excitation input power).

The absorption at 398.8 nm and the emission at 575 nm correspond to the $^6H_{15/2} \rightarrow {}^4F_{7/2}+{}^4I_{13/2}$ and $^4F_{9/2} \rightarrow {}^6H_{13/2}$ of Dy^{3+} is shown in Fig. 3. The input–output characteristics of the Dy:WPFG fiber laser at 575 nm are shown in Fig. 18. The maximum output power was 10.3 mW for 72.5 mW of absorbed pump power. The threshold power was measured to be 10.2 mW, and the slope efficiency was calculated to be 17.1%. Limpert et al. have also demonstrated a Dy^{3+}-doped ZBLAN fiber laser at 575 nm [65]. The reported output power was ∼10 mW; however, the threshold was 40 mW and the slope efficiency was 1.5%. Our laser system is 11 times more efficient than previous work. Since the ZBLAN fiber of previous work was 86 cm long with 1000 ppm of Dy^{3+} concentration, there may be considerable optical loss in such a long fiber. On the other hand, because we were able to make a low-loss optical fiber (0.3 dB/m at 532 nm

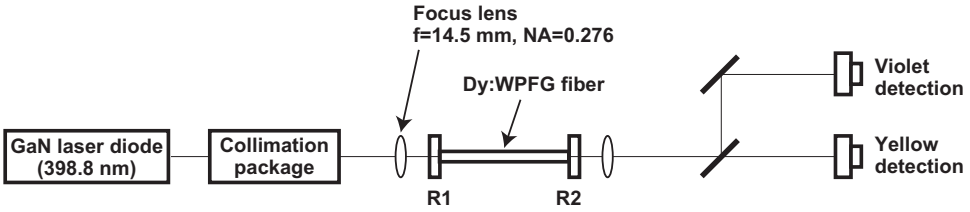

Fig. 17. Setup of laser oscillation experiment for Dy:WPFG fiber.

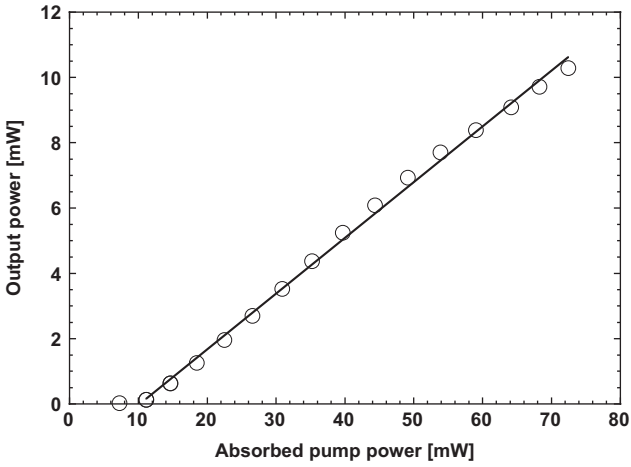

Fig. 18. Input–output characteristics of Dy:WPFG fiber at 575 nm.

[66]) at a higher Dy^{3+} concentration (10,000 ppm), the cavity loss was dramatically decreased. A photograph of the yellow laser while in operation is shown in Fig. 19.

2.5.3. Future prospects

The historical transition of primary red solid-state laser powers is shown in Fig. 20, which summarizes the data in Table 1 and Section 2.5.2. The power available from primary visible solid-state lasers is rapidly increasing because the GaN laser diode power has grown to over 1 W in 3 years. The establishment of waterproof fluoride glass and the fabrication technology of low-loss optical fiber have also played important roles.

In view of photon beam cost, GaN laser diode power will probably be even more significant as an excitation source in the next decade. As research all over the world pursues higher power GaN laser diodes, we will soon have multi-watt GaN laser diodes with multi-emitter array structured bars, which will be stacked to make hundreds of W modules in the future, in a manner similar to the development of infrared high-power semiconductor lasers. Therefore, we believe that the photon cost will be dramatically reduced by mass production.

On the other hand, for photon beam quality, much impressive research on visible lasers is being proposed. The rising power of GaN laser diodes will usher in the same progress in primary visible solid state sources that proceeded the Nd:YAG, or Yb- and Er-doped fiber lasers, and such progress will produce new kinds of visible lasers, including ultra-short pulse lasers such as Ti:sapphire lasers, high-power tunable lasers like dye-lasers, and ultraviolet generation by

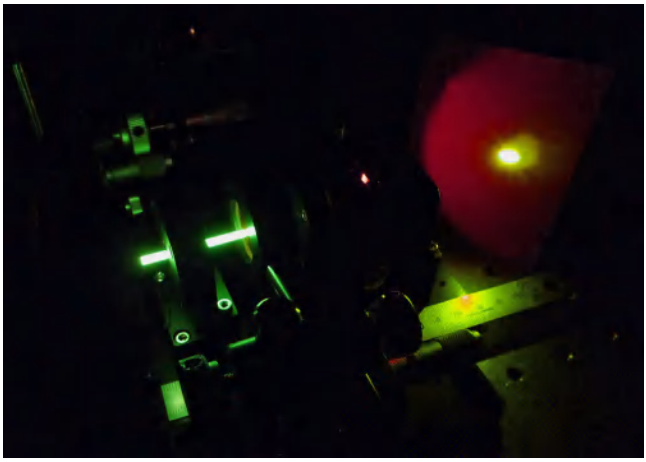

Fig. 19. Photograph of yellow laser oscillation. (For interpretation of the references to color in this figure legend, the reader is referred to the web version of this article.)

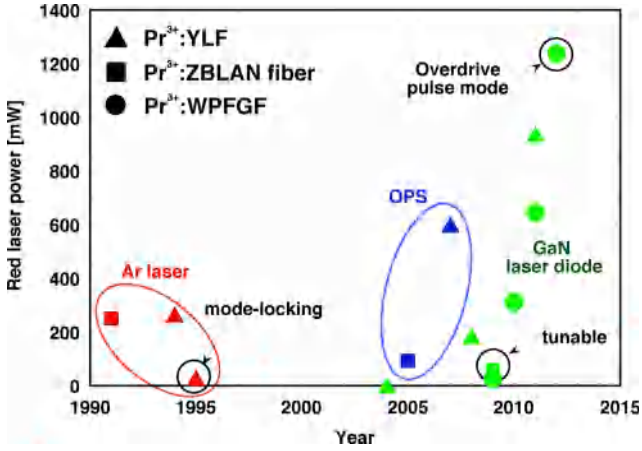

Fig. 20. Historical transition of primary red solid-state laser powers. (For interpretation of the references to color in this figure legend, the reader is referred to the web version of this article.)

second-harmonic generation. The future prospects for visible fiber lasers, pumped by GaN laser diodes, that we project are illustrated in Fig. 21.

2.5.3.1. High-power visible CW laser. In 2012, visible lasers excited by GaN laser diodes and producting at least 1 W of output were demonstrated. Visible lasers are already applicable in many areas, such as display technology, medicine, laser processing, biology, metrology, and optical storage, and we expect visible fiber lasers, which are excited by GaN laser diodes, to be used in such applications. Further research on higher power GaN laser diodes, power combiners, and double-cladding fiber techniques for the visible region will produce a 10 W class of powerful primary visible fiber lasers. Of course, these high-power visible lasers are very useful for

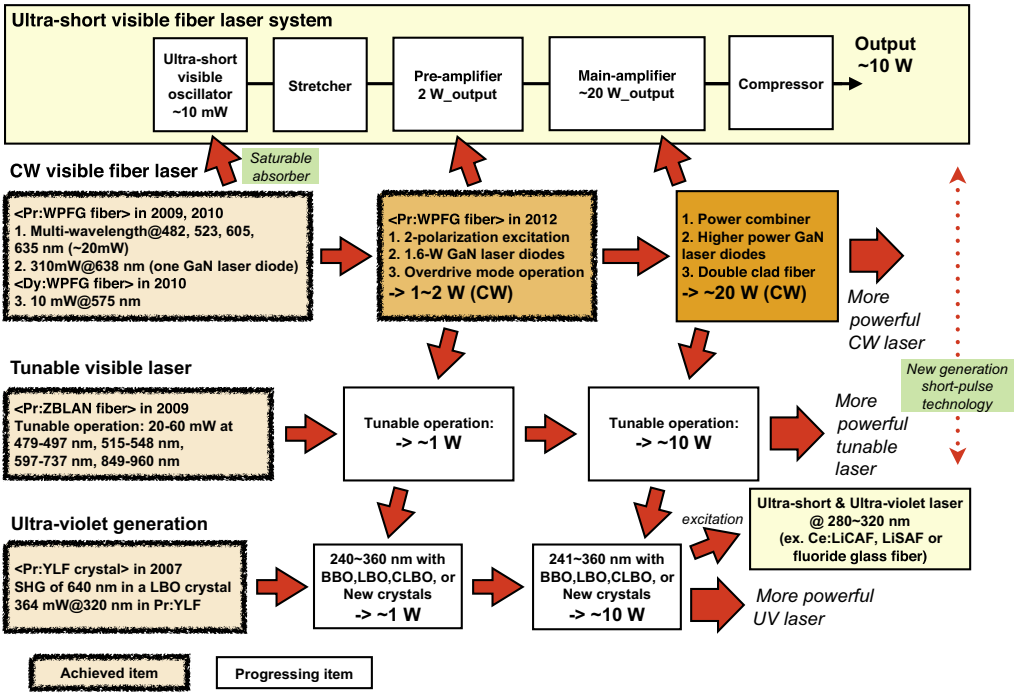

Fig. 21. Future prospects of visible fiber lasers pumped by GaN laser diodes.

industrial uses, including marking, cutting, welding, paste-free soldering. They are also expected to be the light sources for color holograms. For example, although typical copy machines provide only 2-dimensional information on paper, if we combine an appropriate molding machine with a color hologram, we could design a 3-dimensional copy machine. Such a system would be innovative in organ transplant surgery because, if 3-dimensional organ information can be transmitted, doctors can provide more appropriate medical treatment. Of course, 3-dimensional movies with color holograms will enable innovative displays for entertainment markets.

2.5.3.2. High-power tunable visible lasers and ultraviolet generation. Since the visible fiber laser power is increasing, we can easily imagine the appearance of high-power solid-state visible tunable fiber lasers, because, as shown in Table 1, a wide range in tunability was already demonstrated by the Pr:ZBLAN fiber laser [50] when excited by GaN laser diodes. Another fascinating possibility is a compact ultraviolet laser because visible lasers access the ultraviolet region by SHG. Since we often use third- or fourth-harmonic generation (THG or FHG) of Nd:YAG infrared lasers to produce visible ultraviolet radiation, the conversion efficiency of ultraviolet generation from visible lasers is likely to exceed those for THG or FHG. Some SHG trials for visible lasers have been reported, such as an intra-cavity system with a Pr:YLF and a LBO crystal that generates 346 mW at 320 nm [44]. Borate crystals, such as BBO, LBO, and CLBO, are primarily used as SHG crystals for generating visible light. The development of new crystals [98,99] that work in this wavelength region, and a QPM structure in BBO or quartz [100], are strongly desired for obtaining high beam quality in the ultraviolet region. If we get such high quality

ultraviolet lasers, we can use them as an excitation source for Ce:LiCAF, Ce:LiSAF, or Ce-doped fluoride glass fiber to generate a ultrashort pulse in the ultraviolet region [101].

2.5.3.3. Ultrashort visible fiber laser system. Fluoride glass materials display broad fluorescence spectra (Figs. 9 and 11). Based on this property, we made a visible ultrashort pulse laser with a mode-locking technique. Although a mode-locked laser based upon a primary visible solid-state laser was already achieved using Pr:YLF [41,42], the wider fluorescence spectra derived from an inhomogeneous crystal field in glass host materials can produce a shorter pulse duration. The structure of the primary visible solid-state laser will also simplify the ultrashort pulse laser system more than those realized with dye lasers or OPOs. To generate an ultrashort pulse, appropriate saturable absorbers are indispensable. There are numerous candidates for saturable absorbers, such as, laser dyes, semiconductor saturable absorber mirrors (SESAMs) [102], carbon nano-tubes [103], and graphenes [104]. As the research on saturable absorbers progresses in the visible region, a primary ultrashort visible fiber laser will be suitably designed, and research using such ultrashort visible fiber lasers will expand.

The waterproof fluoride glass fiber that we have described will be very useful for practical uses due to its higher tolerance to humidity than is ZBLAN glass. The use of WPFG will to expand other ionic elements, including other rare-earth elements or transition metals, and lasers using new ionic elements will fill the between wavelength Pr:WPFG and Dy:WPFG fiber lasers. Therefore, the primary visible solid-state laser is expected to be a simple, rigid, highly efficient, and low-cost apparatus that will successfully combine the quality and quantity of photon beams in a single laser system.

3. Summary

We have described the status of visible fiber lasers excited by GaN laser diodes, especially the Pr and Dy:WPFG fiber lasers, with a brief review of previously developed visible lasers. We have demonstrated over 1 W operation of Pr:WPFG fiber lasers. Although many types of lasers now exist in the visible region in the gas, liquid, and solid-state phases, the visible fiber lasers excited by GaN laser diodes appear to be advantageous with respect to previous visible lasers in many respects. Of course, the progress of visible fiber lasers was greatly helped by the development of high-power GaN laser diodes and optical fibers of Pr or Dy:WPFG having losses of 0.1–0.3 dB/m (the same as a commercial ZBLAN fiber). This technology will continue to be fueled by the development of double-clad fibers of rare-earth doped WPFG, power combiners for GaN laser diodes, and saturable absorbers for ultrashort pulse generation.

The configuration of primary visible fiber lasers promises highly efficient, cost-effective, and simple laser systems that yield photon beams of high quality but will also lead to new CW or tunable laser systems, compact ultraviolet lasers, and low-cost ultrashort pulse laser systems. We believe that primary visible fiber lasers will be effective tools for creating the next generation of light sources and new areas of research.

Acknowledgments

This work is the product of many researchers. The high-power GaN laser diodes for excitation sources were provided by Nichia Corporation, and many other experimental verifications were made possible by student researchers in Dr. Fujimoto's laboratory. The authors are grateful to everyone who joined in this work for every aspect of their cooperation.

References

[1] ASTM G173-03(2008) Standard Tables for Reference Solar Spectral Irradiances: Direct Normal and Hemispherical on 37° Tilted Surface, ASTM International, West Conshohocken, PA, 2008.
[2] A. Einstein, Physikalische Zeitschrift 18 (1917) 121–128.
[3] A.L. Schawlow, C.H. Townes, Physical Review 112 (1958) 1940–1949.
[4] T.H. Maiman, Nature 187 (1960) 493–494.
[5] W.B. Bridges, Applied Physics Letters 4 (1964) 128–130.
[6] H. Marantz, R.I. Rudko, C.L. Tang, IEEE Journal of Quantum Electronics Qe 5 (1969) 38-&.
[7] A.D. White, J.D. Rigden, Proceedings of the Institute of Radio Engineers 50 (1962) 1697.
[8] A.D. White, E.I. Gordon, J.D. Rigden, Applied Physics Letters 2 (1963) 91–93.
[9] D.L. Perry, IEEE Journal of Quantum Electronics Qe 7 (1971) 102.
[10] W.H. Long, M.J. Plummer, E.A. Stappaerts, Applied Physics Letters 43 (1983) 735–737.
[11] J.W. Gerritsen, A.L. Keet, G.J. Ernst, W.J. Witteman, Journal of Applied Physics 67 (1990) 3517–3519.
[12] W.K. Bischel, H.H. Nakano, D.J. Eckstrom, R.M. Hill, D.L. Huestis, D.C. Lorents, Applied Physics Letters 34 (1979) 565–567.
[13] F.K. Tittel, M. Smayling, W.L. Wilson, G. Marowsky, Applied Physics Letters 37 (1980) 862–864.
[14] F.K. Tittel, W.L. Wilson, R.E. Stickel, G. Marowsky, W.E. Ernst, Applied Physics Letters 36 (1980) 405–407.
[15] I.V. Chaltakov, N.I. Minkovsky, I.V. Tomov, Optics Communications 65 (1988) 33–36.
[16] W.T. Silfvast, G.R. Fowles, B.D. Hopkins, Applied Physics Letters 8 (1966) 318–319.
[17] W.T. Silfvast, New Cw Metal-Vapor Laser, Applied Physics Letters 15 (1969) 23-&.
[18] A.K. Anders, E.C. Harvey, R.C. Tobin, Applied Physics Letters 49 (1986) 923–924.
[19] D.W. Coutts, M.D. Ainsworth, J.A. Piper, Optics Communications 75 (1990) 301–306.
[20] D.N. Astadjov, K.D. Dimitrov, D.R. Jones, V.K. Kirkov, C.E. Little, N.V. Sabotinov, N.K. Vuchkov, IEEE Journal of Quantum Electronics 33 (1997) 705–709.
[21] H. Kimura, N. Aoki, C. Konagai, S. Shirayama, T. Miyazawa, Journal of Nuclear Science and Technology 31 (1994) 34–47.
[22] B.H. Soffer, Applied Physics Letters 10 (1967) 266–267.
[23] M.J. Weber (Ed.), CRC Handbook of Laser Science and Technology, Supplement 1: Lasers, CRC Press, Inc., Boca Raton, FL, 1991.
[24] A. Dienes, Opto-Electronics 6 (1974) 99–113.
[25] F.N. Baltakov, B.A. Barikhin, L.V. Sukhanov, JETP Letters 19 (1974) 174–175.
[26] F.P. Schafer, W. Schmidt, J. Volze, Applied Physics Letters 9 (1966) 306–309.
[27] F. Salin, G. Lesaux, P. Georges, A. Brun, C. Bagnall, J. Zarzycki, Optics Letters 14 (1989) 785–787.
[28] Y.X. Fan, R.C. Eckardt, R.L. Byer, J. Nolting, R. Wallenstein, Applied Physics Letters 53 (1988) 2014–2016.
[29] W.R. Bosenberg, L.K. Cheng, C.L. Tang, Applied Physics Letters 54 (1989) 13–15.
[30] R. Scheps, Progress in Quantum Electronics 20 (1996) 271–358.
[31] D.S. Funk, J.G. Eden, in: M.J.F. Digonnet (Ed.), Rare-Earth-Doped Fiber Lasers and Amplifiers, CRC Press, New York, 1993.
[32] Y. Hirano, Highly Efficient, Compact Green Laser for Laser TV, LASE, Part of SPIE Phonotics West 2009 San Jose Convention center, San Jose, CA, USA, 2009, pp. 7902–7913.
[33] A. Obana, Laser Eng. 29 (2001) 438–444.
[34] J. Francis, A. L'Esperance, Ophthalmic Lasers, Mosby, St. Louis, 1989.
[35] W. Koechner, Solid-state Laser Engineering, Springer, New York, 2006.
[36] A.K. Burnham, UCRL-LR-105821-000099-000002, Producing KDP and DKDP Crystals for the NIF Laser, ICF Quarterly Report, January–March 1999, vol. 9 (2), Lawrence Livermore National Laboratory, 1999.
[37] S.V. Tovstonog, S. Kurimura, K. Kitamura, Applied Physics Letters 90 (2007) 051115.
[38] R.G. Smart, J.N. Carter, A.C. Tropper, D.C. Hanna, S.T. Davey, S.F. Carter, D. Szebesta, Optics Communications 86 (1991) 333–340.
[39] R.G. Smart, D.C. Hanna, A.C. Tropper, S.T. Davey, S.F. Carter, D. Szebesta, Electronics Letters 27 (1991) 1307–1309.
[40] T. Sandrock, T. Danger, E. Heumann, G. Huber, B.H.T. Chai, Applied Physics B—Lasers and Optics 58 (1994) 149–151.
[41] S. Ruan, J.M. Sutherland, P.M.W. French, J.R. Taylor, B.H.T. Chai, Optics Letters 20 (1995) 1041–1043.
[42] J.M. Sutherland, P.M.W. French, J.R. Taylor, B.H.T. Chai, Optics Letters 21 (1996) 797–799.

[43] A. Richter, H. Scheife, E. Heumann, G. Huber, W. Seelert, A. Diening, Electronics Letters 41 (2005) 794–795.
[44] A. Richter, E. Heumann, G. Huber, V. Ostroumov, W. Seelert, Optics Express 15 (2007) 5172–5178.
[45] A. Richter, E. Heumann, E. Osiac, G. Huber, W. Seelert, A. Diening, Optics Letters 29 (2004) 2638–2640.
[46] P. Camy, J.L. Doualan, R. Moncorge, J. Bengoechea, U. Weichmann, Optics Letters 32 (2007) 1462–1464.
[47] F. Cornacchia, A. Di Lieto, M. Tonelli, A. Richter, E. Heumann, G. Huber, Optics Express 16 (2008) 15932–15941.
[48] T. Gun, P. Metz, G. Huber, Optics Letters 36 (2011) 1002–1004.
[49] F. Cornacchia, A. Richter, E. Heumann, G. Huber, D. Parisi, M. Tonelli, Optics Express 15 (2007) 992–1002.
[50] H. Okamoto, K. Kasuga, I. Hara, Y. Kubota, Optics Express 17 (2009) 20227–20232.
[51] H. Okamoto, K. Kasuga, Y. Kubota, Optics Letters 36 (2011) 1470–1472.
[52] Y. Fujimoto, O. Ishii, M. Yamazaki, Electronics Letters 45 (2009) 1301–1302.
[53] J. Nakanishi, T. Yamada, Y. Fujimoto, O. Ishii, M. Yamazaki, Electronics Letters 46 (2010) 1285–1286.
[54] J. Nakanishi, T. Yamada, Y. Fujimoto, O. Ishii, M. Yamazaki, CJp6, Sub-watt output power at 638 nm in wavelength by direct oscillation with Pr-doped waterproof fluoro-aluminate glass fiber laser, in: 2011 Conference on Lasers and Electro-Optics Europe and 12th European Quantum Electronics Conference (CLEO®/Europe—EQEC 2011), IEEE Conference Publications Operations, ICM—International Congress Centre, Munich, Germany, 2011.
[55] J. Nakanishi, Y. Horiuchi, T. Yamada, O. Ishii, M. Yamazaki, M. Yoshida, Y. Fujimoto, Optics Letters 36 (2011) 1836–1838.
[56] D.Y. Wang, Y.Y. Guo, G.H. Sun, H. Li, L. Zhao, G.P. Xu, Journal of Alloys and Compounds 451 (2008) 122–124.
[57] T. Omatsu, A. Lee, H.M. Pask, J. Piper, Applied Physics B-Lasers and Optics 97 (2009) 799–804.
[58] J. Ota, A. Shirakawa, K. Ueda, Japanese Journal of Applied Physics Part 2—Letters & Express Letters 45 (2006) L117–L119.
[59] E.M. Dianov, A.V. Shubin, M.A. Melkumov, O.I. Medvedkov, I.A. Bufetov, Journal of the Optical Society of America B—Optical Physics 24 (2007) 1749–1755.
[60] M. Fallahi, L. Fan, Y. Kaneda, C. Hessenius, J. Hader, H. Li, J.V. Moloney, B. Kunert, W. Stolz, S.W. Koch, J. Murray, R. Bedford, IEEE Photonics Technology Letters 20 (2008) 1700–1702.
[61] S.E. McCoy, Lasers in Surgery and Medicine 21 (1997) 329–340.
[62] S. Tanabe, T. Hanada, M. Watanabe, T. Hayashi, N. Soga, Journal of the American Ceramic Society 78 (1995) 2917–2922.
[63] D. Parisi, A. Toncelli, M. Tonelli, E. Cavalli, E. Bovero, A. Belletti, Journal of Physics-Condensed Matter 17 (2005) 2783–2790.
[64] M. Higuchi, R. Sasaki, J. Takahashi, Journal of Crystal Growth 311 (2009) 4549–4552.
[65] J. Limpert, H. Zellmer, P. Riedel, G. Maze, A. Tunnermann, Electronics Letters 36 (2000) 1386–1387.
[66] Y. Fujimoto, O. Ishii, M. Yamazaki, Electronics Letters 46 (2010) 586–587.
[67] G.H. Dieke, H.M. Crosswhite, Applied Optics 2 (1963) 675–686.
[68] A.A. Kaminskii, Laser Crystals: Their Physics and Properties, Springer-Verlag, Berlin, 1990.
[69] W.T. Carnall, P.R. Fields, K. Rajnak, Journal of Chemical Physics 49 (1968) 4424–4442.
[70] M.J. Weber, Journal of Chemical Physics 48 (1968) 4774–4780.
[71] M. Shojiya, M. Takahashi, R. Kanno, Y. Kawamoto, K. Kadono, Journal of Applied Physics 82 (1997) 6259–6266.
[72] J.C. Joshi, N.C. Pandey, B.C. Joshi, B.C. Pandey, J. Joshi, Solid State Communications 27 (1978) 1051–1053.
[73] V.M. Goldschmidt, Skrifter Norske Videnskaps Akademi i Oslo, vol. 8, 1926, 127 pp.
[74] M.J. Weber, C.B. Layne, R.A. Saroyan, D. Milam, Optics Communications 18 (1976) 171–172.
[75] M.J. Weber, C.F. Cline, R.A. Saroyan, D. Milam, W.L. Smith, G.J. Linford, S.E. Stokowski, W.F. Hagen, C. B. Layne, C.M. Baldwin, Journal of the Optical Society of America 68 (1978) 542–542.
[76] C.M. Baldwin, R.M. Almeida, J.D. Mackenzie, Journal of Non-Crystalline Solids 43 (1981) 309–344.
[77] M. Poulain, M. Poulain, J. Lucas, Materials Research Bulletin 10 (1975) 243–246.
[78] T. Iqbal, M.R. Shahriari, G. Merberg, G.H. Sigel, Journal of Materials Research 6 (1991) 401–406.
[79] Y. Wang, N. Sawanobori, S. Nagahama, Journal of Non-Crystalline Solids 128 (1991) 322–325.
[80] S. Mitachi, T. Manabe, Japanese Journal of Applied Physics 19 (1980) L313–L314.
[81] T. Iqbal, M.R. Shahriari, R. Ulbrich, G.H. Sigel, Optics Letters 16 (1991) 1611–1613.
[82] D. Szebesta, S.T. Davey, J.R. Williams, M.W. Moore, Journal of Non-Crystalline Solids 161 (1993) 18–22.
[83] G.P. Agrawal, Nonlinear Fiber Optics, Academic Press Inc., San Diego, 1995.
[84] S. Calvez, J.E. Hastie, M. Guina, O.G. Okhotnikov, M.D. Dawson, Laser & Photonics Reviews 3 (2009) 407–434.
[85] J.L. Chilla, S.D. Butterworth, A. Zeitschel, J.P. Charles, A.L. Caprara, M.K. Reed, a.L. Spinelli, Proceedings of SPIE 143 (2004) 5332.
[86] J. Chilla, Q.-Z. Shu, H. Zhou, E. Weiss, M. Reed, L. Spinelli, Proceedings of SPIE 6451 (2007) 645109.

[87] J. Rautiainen, A. Harkanen, V.M. Korpijarvi, P. Tuomisto, M. Guina, O.G. Okhotnikov, Optics Express 15 (2007) 18345–18350.
[88] S. Ishizawa, K. Kishino, R. Araki, A. Kikuchi, S. Sugimoto, Applied Physics Express 4 (2011).
[89] D. Sands, Diode Lasers, Institute of Physics Publishing, Bristol and Philadelphia, 2005.
[90] M. Ikeda, M. Honda, Y. Mori, K. Kaneko, N. Watanabe, Applied Physics Letters 45 (1984) 964–966.
[91] I. Hino, S. Kawata, A. Gomyo, K. Kobayashi, T. Suzuki, Applied Physics Letters 48 (1986) 557–558.
[92] S. Nakamura, T. Mukai, M. Senoh, Applied Physics Letters 64 (1994) 1687–1689.
[93] D. Queren, A. Avramescu, G. Bruderl, A. Breidenassel, M. Schillgalies, S. Lutgen, U. Strauss, Applied Physics Letters 94 (2009) 081119.
[94] J.W. Raring, M.C. Schmidt, C. Poblenz, Y.C. Chang, M.J. Mondry, B. Li, J. Iveland, B. Walters, M.R. Krames, R. Craig, P. Rudy, J.S. Speck, S.P. DenBaars, S. Nakamura, Applied Physics Express, 3, 112101.
[95] Y.E. Shimpei Takagi, Takashi Kyono, Masahiro Adachi, Yusuke Yoshizumi, Takamichi Sumitomo, Yuichiro Yamanaka, Tetsuya Kumano, Shinji Tokuyama, Kazuhide Sumiyoshi, Nobuhiro Saga, Masaki Ueno, Koji Katayama, Takatoshi Ikegami, Takao Nakamura, Katsunori Yanashima, Hiroshi Nakajima, Kunihiko Tasai, Kaori Naganuma, Noriyuki Fuutagawa, Yoshiro Takiguchi, Tatsushi Hamaguchi, Masao Ikeda, Applied Physics Express 5 (2012) 082102.
[96] J. Kasai, R. Akimoto, T. Hasama, H. Ishikawa, S. Fujisaki, S. Tanaka, S. Tsuji, Applied Physics Express 4 (2011) 082102.
[97] S. Adachi, Journal of Applied Physics 102 (2007) 063502.
[98] K. Shimamura, E.G. Villora, H.R. Zeng, M. Nakamura, S. Takekawa, K. Kitamura, Applied Physics Letters 89 (2006) 232911.
[99] E.G. Villora, K. Shimamura, K. Sumiya, H. Ishibashi, Optics Express 17 (2009) 12362–12378.
[100] S. Kurimura, M. Harada, K. Muramatsu, M. Ueda, CTuL1, Quasi-phase-matched second-harmonic generation at vacuum ultraviolet 193 nm, in: Proceedings of the Conference on Lasers and Electro-Optics (CLEO)/The International Quantum Electronics Conference (IQEC), Optical Society of America, Baltimore Convention Center, Baltimore, MD, USA, 2011.
[101] E. Granados, D.W. Coutts, D.J. Spence, Optics Letters 34 (2009) 1660–1662.
[102] V.G. Savitski, I.M. Ranieri, A.B. Krysa, S. Calvez, CMB7, Passively Q-switched Pr:YLF laser, in: Proceedings of the Conference on Lasers and Electro-Optics (CLEO)/The International Quantum Electronics Conference (IQEC), Optical Society of America, Baltimore Convention Center, Baltimore, MD, USA, 2011.
[103] S.Y. Set, H. Yaguchi, Y. Tanaka, M. Jablonski, IEEE Journal of Selected Topics in Quantum Electronics 10 (2004) 137–146.
[104] Q.L. Bao, H. Zhang, Y. Wang, Z.H. Ni, Y.L. Yan, Z.X. Shen, K.P. Loh, D.Y. Tang, Advanced Functional Materials 19 (2009) 3077–3083.